Numerical Analysis of Pressure on Cup Surface after THA

Shin KAI[1], Makoto SAKAMOTO[2], Koichi KOBAYASHI[2], Izumi MINATO[3], Yoshio KOGA[4] and Yuji TANABE[5]

[1]Graduate School of Science and Technology, Niigata University, Niigata 950-2181, Japan
[2]Department of Health Sciences, Niigata University School of Medicine, Niigata, Japan
[3]Department of Orthopedics, Niigata Rinko Hospital, Niigata, Japan
[4]Department of Orthopedics, Niigata Kobari Hospital, Niigata, Japan
[5]Department of Mechanical and Production Engineering, Niigata University, Niigata, Japan

Abstract

Estimation of the artificial hip joint contact area and pressure distribution during motions of daily life is important in predicting joint degeneration mechanism and implant wear. The purpose of this study was to develop a method of applying discrete element analysis (DEA) based on a rigid body spring model to artificial hip joint, and to analyze contact area and pressure distribution during different motions. Post-operative motion analyses of four basic motions, such as fast walking, slow walking, standing up and sitting down were performed by using VICON system and Kistler force plate. Implant orientation was obtained by matching the contours of 3D bone model and implant CAD model to those of the biplanar CR images. Triangular mesh at interior surface of cup model was considered as liner surface and used for applying DEA to artificial hip joint. Because stem model was considered to be a rigid body and consequential transformations occurred only inside the liner model, triangular mesh was considered to be a compressive spring respectively. The change of contact area and the pressure distribution under dynamic condition were calculated easily through these considerations, and rapid increase accompanied with change of area was observed in knee bending motions.

Key words

THA, Artificial Hip Joint, Discrete Element Analysis, Rigid Body Spring Model, Contact Area, Pressure Distribution

1. Introduction

Total hip arthroplasty (THA), also hip replacement, is a surgical procedure in which the hip joint is replaced by a prosthetic implant. The modern and widely known artificial hip joint was developed by John Charnley in the 1970s [1], and consisted of three parts, 1. a metallic femoral stem, 2. a UHMWPE acetabular liner, 3. a metallic acetabular socket or bone cement. Acetabular liner has a bearing surface of UHMWPE which has a low coefficient of friction and low wear rate. In the long term, wear particulate dose accumulate and lead to a condition known as osteolysis, which leads to bone loss, joint loosening, discomfort, and ultimately limits the lifespan of the artificial joint [2,3]. Therefore, the evaluation of the wear on acetabular bearings, which depends directly on contact pressure, is essential to analyze the failure of the acetabular implant, as well as for a better design of artificial joint.

Some authors have presented computational models such as finite element analysis (FEA) to analyze the hip joint, in order to study either the wear or the pressure distribution [4-

8]. Due to the long calculating time of FEA, more simple methods such as elasticity analyses and elastic foundation analyses were performed to predict contact pressure [9,10], but usually only under static conditions.

Discrete element analysis (DEA) based on a rigid body spring model (RBSM) is an efficient numerical tool, which provides a near real-time computational result [11,12]. The accuracy of the technique was confirmed with other methods, including FEA, in the quantification of the contact stress [10,13]. Therefore we can perform a quasi-static analysis under dynamic condition using DEA technique. The purpose of this study is to develop a method of applying DEA based on RBSM to artificial hip joint, and to analyze the contact area and pressure distribution on bearing surface during different motions of daily life.

2. Materials and Methods

2.1 Post-operative motion analysis

Analysis of pressure distribution and contact area requires boundary condition including hip contact forces and relative positions between acetabular implant and femoral implant. Post-operative motion analysis was performed to obtain these data.

One patient (sex: female, age: 81yrs, weight: 650 N) after THA was analyzed. 3D geometric bone model (3DGBM) of pelvis and femur was reconstructed from CT volume images using a 3D visualization and modeling software (ZedView, LEXI, Inc, Tokyo, Japan). The anatomical coordinate systems were established on the 3DGBM according to the following definitions. Each coordinate system of the pelvis and femur was based on 3 discrete points on the 3DGBM. These points were the bilateral anterior superior iliac spines and the pubic symphysis (RASIS, LASIS, and PUB, respectively) for the pelvis, and the center of femoral head, centers of medial and lateral posterior condyles obtained by spherical approximation (CFH, CMPC, and CLPC, respectively) for the femur (Fig.1). The Unit vectors of the pelvic and femoral coordinate system were defined as follows. For the pelvis, the X axis was parallel to the line that included RASIS and LASIS; Y axis was perpendicular to the plane that included RASIS, LASIS, and PUB (that is, the anatomical pelvic plane); Z axis was perpendicular to the X and Y axes, and PUB was set as the origin. For the femur, the X axis was parallel to the line that included CMPC and CLPC; Y axis was perpendicular to the plane that included CMPC, CLPC, and CFH; Z axis was perpendicular to the X and Y axes, and the midpoint between CMPC and CLPC was set as the origin.

Biplanar AP and 60 deg. Oblique long-leg (from the pelvis to the ankle joint) CR projections were performed simultaneously. A camera calibration procedure that calculates a projection matrix to determine the 3D position in space of objects from biplanar CR images was performed in advance [14]. 3DGBM of either bone was projected onto the AP and 60 deg. Oblique CR images using the projection matrix, and Computer-aided design (CAD) data of the implant was projected also. By matching the silhouettes of these digital models to the contours of the respective bone images and implant images on the CR images through 3D rotation and translation, the 3D position and alignment of the implants relative to the pelvis and femur can be computed (Fig.2).

The results of implant orientation were presented in Table 1. The cup size was 52 mm, and the head size was 26mm. The thickness of liner was 9mm. The angles of inclination and anteversion determined by three methods were calculated based on pelvic coordinate system [15], and femoral anteversion was calculated based on femoral coordinate system [16].

To obtain the motional data, instrumented femoral head prostheses have been used to investigate the magnitude, direction, and moment of the hip contact forces during motions of daily life [17]. These direct measurements of the hip contact force can provide the accurate loading conditions
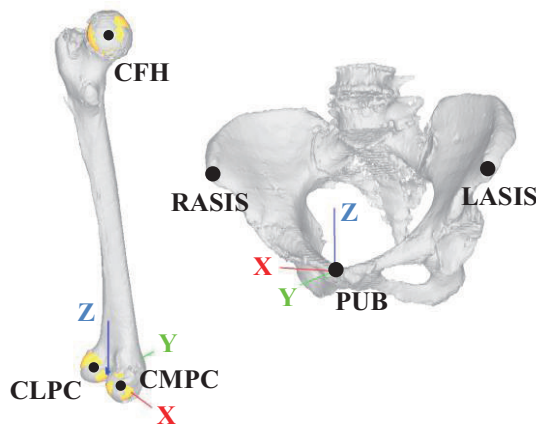

Fig.1 Definitions of the pelvic and femoral coordinate systems. RASIS and LASIS indicate the most anterior points of the right and left anterior superior iliac spine; PUB, the most anterior point of the pubic symphysis; CMPC and CLPC, the centers of spheres representing the medial and lateral posterior condyles; CFH, the center of femoral head.

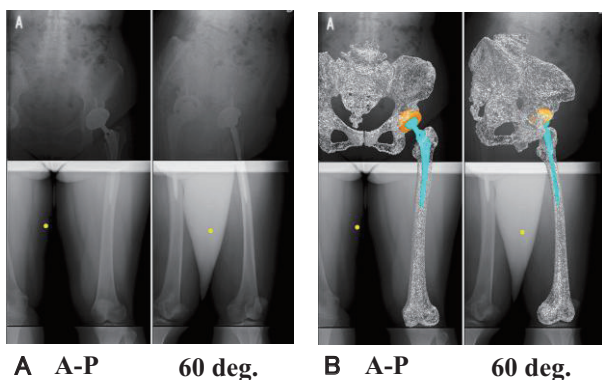A A-P   60 deg.   B A-P   60 deg.

Fig.2 (A) Post-operative biplanar CR images (AP and 60 deg.). (B) The projected images of each digital model were matched respectively.

required by the DEA method. Thus, we reproduced four post-operative motions by applying average values of these measurements to our patient (Table 2). Standing up motion was represented in Fig.3 as an example.

Table 1 Results of implant orientation, AA, OA, and RA indicate the anatomical anteversion, operative anteversion, and radiographic anteversion; RI indicates radiographic inclination measured on coronal plane of pelvic coordinate system; FA indicates femoral anteversion measured on axial plane of femoral coordinate system.

AA [deg.]	OA [deg.]	RA [deg.]	RI [deg.]	FA [deg.]
31.21	26.23	20.92	39.12	26.47

Table 2 Reproduced motions

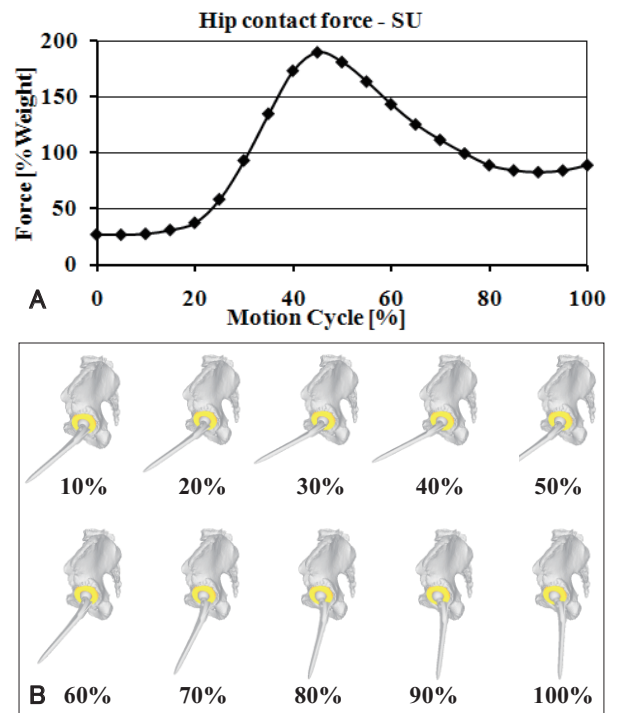| Motion	Abbreviation	Description
Slow Walking	SW	Level ground, speed = 0.98 m/s
Fast Walking	FW	Level ground, speed = 1.46 m/s
Standing Up	SU	chair height = 50 cm
Sitting Down	SD	chair height = 50 cm

Fig.3 (A) Hip contact force, (B) Relative position between the pelvis and the stem, were reproduced during standing up motion.

2.2 Discrete element analysis
Boundary condition including hip contact forces and relative positions was obtained by post-operative motion analysis. Because these analyses were performed under dynamic condition, boundary data were serial data, and always changeable during each motion cycle. To enable a quasi-static analysis, an interpolation of the measurements was

finally performed so that the cycle of each motion consisted of 201 equidistant segments. Then DEA method was applied in each segment.

As a preparation of DEA, the stem head was considered to be a rigid body and consequential deformations occurred only inside the liner according to RBSM. Interior surface of cup model consisted of triangular fine mesh was considered as the liner surface, and exterior surface was considered fixed. The liner surface was divided into 22752 triangles, and an imaginary compressive spring was placed on each mesh to model the elastic deformation. The stiffness of the compressive spring was determined from the UHMWPE Young's modulus E of 940 MPa [18], Poisson's ratio ν of 0.46, and liner thickness H. Then coordinate transformation with respect to setting Z axis of whole model in the direction of the hip contact force at each segment was performed.

When the hip contact force F was applied through the stem head, liner surface began to deform, and stem head penetrated the liner surface analytically [Fig.4]. Thus, iterative calculation was performed to estimate the area of deformation. The clearance of penetration δ_i in each mesh can be expressed by the following Eq. (1), if imaginary transformation T was applied along the Z axis.

$$\delta_i = N_{Si} + T - N_{Ci} \qquad (1)$$

the spring placed on each mesh was used to model the deformation, and the compressive stress σ_i of each mesh can be calculated by following Eq. (2):

$$\sigma_i = \frac{E(1-\nu)}{(1+\nu)(1-2\nu)} \cdot \frac{\delta_i}{H_i} \qquad (2)$$

where H_i was the liner thickness at the spring location, and calculated separately for each spring as the local liner thickness in the superior-inferior direction. Finally, iteration was continued until total force F_t exerted by all springs was equal to the hip contact force F at current segment. The total force F_t can be calculated by following Eq. (3):

$$F_t = \sum_{i=1}^{N} \sigma_i \cdot A_i \qquad (3)$$

where N was the sum of deformed mesh, and A_i indicates the projected area of each mesh on the plane perpendicular to the Z axis.

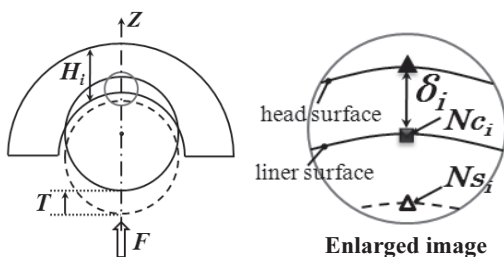The compressive stresses obtained from this process across the bearing surface can be regarded as the joint

Fig.4 2D sketch of the penetration, T indicates the translation of the stem head; N_{Ci} and N_{Si} indicate the nodes of an arbitrary contact pair (mesh No. i), and the stem head

was considered as a sphere; δ_i indicates the clearance of penetration in current pair.
contact pressure distribution, and can be transformed to the normal direction easily. It is possible to estimate not only the pressure values but also the contact area as the sum of the deformed mesh.

3. Results
The peak pressure, contact area, and location where peak pressure was observed were summarized in Table 3 for each motion of daily life (Table 2). The contact area was calculated as ratio of total liner surface.

For two walking motions, the 0% motion cycle was defined at heel-contact of the leg and 100% was defined at the instant just before the second heel-contact of the ipsilateral leg. The two peaks in contact pressure were observed with a maximum value of 11.42 MPa and the corresponding contact area was 25.5% during fast walking. Similar configuration can be seen in the slow walking, and peak pressure was lower than fast walking (Fig.5 (A)).

For standing up motion, the full cycle was defined from hip-off to standing. Rapid increase accompanied with change of area was observed, the maximum pressure was 14.81 MPa at the instant just before the extension of the stem (Table 3 and Fig.3 (B) (C)). Similar rapid change can be seen in sitting down motion, the peak pressure was 13.23 MPa, and the change of contact area was contrary to standing up motion (Fig.5 (B)).

The pressure distribution and contact area during standing up motion were visualized in Fig.5 (C). Small contact area at the edge of the superior liner surface was observed during flexed posture, and the same phenomenon can be seen in the sitting down motion.

Table 3 Results of peak pressure, corresponding contact area, and location.

Motion	Peak Pressure [Mpa}	Contact Area [%LinerSurface]	Motion Cycle [%]
Slow Walking	11.21	26.0	18.0
Fast Walking	11.42	25.5	16.5
Standing Up	14.81	16.4	46.0
Sitting Down	13.23	15.3	48.0

4. Discussion
Pre-operative planning and post-operative evaluation for THA are usually performed to estimate implant orientation, ROM (range of motion), and dislocation. Because wear particulate generated on bearing surface causes many serious problems after THA, pressure distribution on bearing surface should also be considered in both processes. This study presented an attempt to analyze the pressure distribution of the liner surface in vivo under dynamic condition. The advantage of DEA technique was short calculating time. Simple assumptions based on RBSM provided a near real time calculation, and the pressure distribution was obtained during each motion. This method enabled both processes to evaluate the condition of contact between implants efficiently.
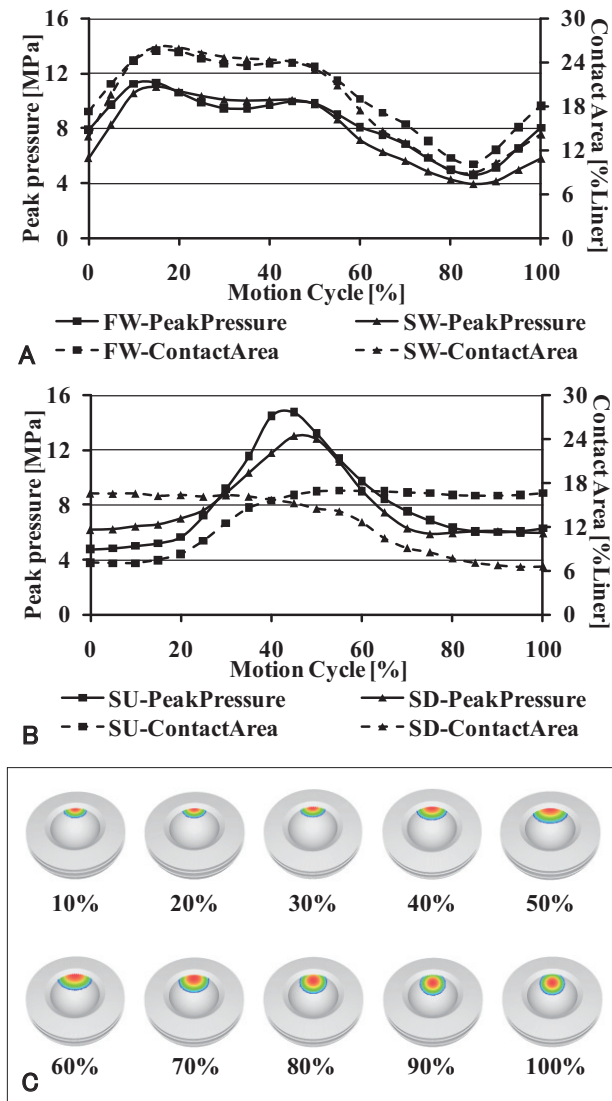
Fig.5 (A) Peak contact pressure and contact area during slow walking and fast walking. (B) Peak contact pressure and contact area during standing up and sitting down. (C) Pressure distribution and contact area during standing up.

Contact areas of four motions existed on superior liner surface, the highest pressure occurred in standing up motion. The pressure distribution concentrated at the edge of surface during fixed posture, this may lead to fracture in the long term.

For the estimation of the pressure distribution, it is important and well-known to calculate the pressure distribution using a dynamic procedure under a dynamic boundary condition. So far dynamic FEA has been usually used. While the dynamic boundary condition can be obtained by performing the post-operative motion analysis, the dynamic procedure of such model is very complicated. There are not only problems of calculating time but also some technical problems of modeling. For our hip model, we have to move acetabular implant while calculating. Then the magnitude and direction of force is always changeable. It is complicated and uncertain to define such boundary condition unless define the model as a rigid body

[19,20]. If our quasi-static analyses can match dynamic results obtained from dynamic procedure, this technique would be chosen as a simple method for estimation of pressure. So the comparison with dynamic FEA would be our next scheme.

Limitations are also present in this method. First, the contact model is static and elastic model, and does not account for visco-elasticity of UHMWPE. A visco-elastic model would require the serial track of deformation, and make model more complicated. Precisely, strain rate determining the visco-elastic property differs variously at each motion, and has much difficulty to unify. Second, this method provides pressure distribution at only liner surface, estimation including sub-surface stresses would require FEA.

5. Conclusion
We developed a method to apply DEA technique to artificial hip joint. The pressure distribution and contact area were calculated at four motions. High pressure distribution was observed at flexion/extension motions.

References
[1] Charnley, J.: Low friction arthroplasty of the hip: theory and practice, *Berlin, etc: Springer-Verlag*, (1987).
[2] J.H. Dumbleton, M.T. Manley, and A.A. Edidin: A literature review of the association between wear rate and asteolysis in total hip arthroplasty, *J. Arthroplasty*, **17**(2002), 649-661.
[3] N.D.L. Burger, P.L. de vaal, and J.P. Meyer: Failure analysis on retrieved ultra high molecular weight polyethylene (UHMWPE) acetabular cups, *Eng Fail Anal*, **14**(2007), 1329-1345.
[4] Bartel, D.L., Bicknell, V.L., and Wright, T.M.: The effect of conformity, thickness, and material on stresses in ultra-high molecular weight components for total joint replacement, *J Bone Joint Surg,* **68-A** (1986), 1041-1051.
[5] Maxian, T.A., Brown, T.D., Pedersen, D.R., and Callaghan, J.J.: A sliding-distance-coupled finite element formulation for polyethylene wear in total hip arthroplasty, *J Biomech*, **29**(1996), 687-692.
[6] Kurts, S.M., Edidin, A.A., and Bartel, D.L.: The role of backside polishing, cup angle, and polyethylene thickness on the contact stresses in metal-backed acetabular components, *J Biomech*, **30**(1997), 639-642.
[7] Tenh, S.H., Chan, W.H., and Thampuran, R.: An elasto-plastic finite element model for polyethylene wear in total hip arthroplasty, *J Biomech*, **35**(2002), 323-330.
[8] Fialho, J.C., Fernandes, P.R., Eca, L. and Folgado, J.: Computational hip joint simulator for wear and heat generation, *J Biomech*, **40**(2007), 2358-2366.
[9] Bartel, E.L., Burstein, A.H., Toda, M.D. and Edwards, D.L.: The effect of conformity and plastic thickness on contact stresses in metal-backed plastic implants, *J Biomech Eng*, **107**(1985), 193-199.

[10] Li, G., Sakamoto, M., and Chao, E.Y.S.: A comparison of different methods in predicting static pressure distribution in articulating joints, *J Biomech*, **30**(1997), 635-638.

[11] Genda, E., Konishi, N., Hasegawa, Y., and Miura, T.: A computer simulation study of normal and abnormal hip joint contact pressure, *Arch Orthop Trauma Surg*, **114**(1995), 202-206.

[12] Genda, E., Iwasaki, N., Li, G., MacWilliams, B.A., Barrance, P.J., and Chao, E.Y.S.: Normal hip joint contact pressure distribution in single-leg standing: effect of gender and anatomic parameters, *J Biomech*, **34**(2001), 895-905.

[13] Sakamoto, M., Li, G., Hara, T., and Chao, E.Y.S.: A new method for theoretical analysis of static indentation test, *J Biomech*, **29**(1996), 679-685.

[14] Sato, T., Koga, Y., and Omori, G.: Three-dimensional lower extremity alignment assessment system: Application to evaluation of component position after total knee arthroplasty, *J Arthroplasty,* **19**(2004), 620-628.

[15] Murray, D.W.: The definition and measurement of acetabular orientation, *J Bone Joint Surg Br,* **75**(1993), 228-232.

[16] Pierchon, F., Pasquier, G., and Cotton, A.: Causes of dislocation of total hip arthroplasty: CT study of component alignment, *J Bone Joint Surg Br,* **76**(1994), 45-48.

[17] Bergmann, G., Deuretzbacher, G., Heller, M., Graichen, F., Rohlmann, A. and Strauss, J.D.: Hip contact forces and gait patterns from routine activities, *J Biomech,* **34**(2001), 859-871.

[18] Bergstrom, J.S., Rimnac, C.M., and Kurtz, S.M.: Prediction of multiaxial mechanical behavior for conventional and highly crosslinked UHMWPE using a hybrid constitutive model, *Biomaterials,* **24**(2003), 1365-1380.

[19] Giddings, V.L., Kurtz, S.M., and Edidin, A.A.: Total knee replacement polyethylene stresses during loading in a knee simulator, *J Tribol,***123**(2001), 842-847.

[20] Godest, A.C., Meaugonin, M., Hang, E., Taylor, M., and Gregson, P.J.: Simulation of a knee joint replacement during a gait cycle using explicit finite element analysis, *J Biomech,* **35**(2002), 267-276.